

OBSERVATION AND NUMERICAL MODELING OF TIDAL SAND DUNE DYNAMICS

Arnaud Doré¹, Philippe Bonneton², Vincent Marieu³ and Thierry Garlan⁴

Abstract

An array of instruments was deployed in the Arcachon tidal inlet, southwest France, to measure sand dune dynamics for two tidal cycles. Based on the measurements, we quantified dune crest horizontal and vertical displacements that show an important dynamics in phase with the tidal currents. We observed superimposed ripples located on dune stoss side and front, migrating on the dune profile and changing polarity as tidal currents reverse. We used a 2D RANS model to simulate the morphodynamic evolution of a flat non-cohesive sand bed submitted to a tidal current. The model reproduces the bed evolution until a field of sand ripples is obtained, that are comparable with observed superimposed ripples in terms of geometrical dimensions and dynamics. We then successfully simulated the dynamics of a field of large sand dunes of similar size as the dunes observed *in situ*. In both cases the simulation results compare well with measurements qualitatively and quantitatively. This research allows for a better understanding of tidal sand dunes and superimposed ripple morphodynamics, and open new perspectives for the use of numerical models to predict their evolution.

Key words: dunes, ripples, sediment transport, morphodynamics, measurements, numerical modeling

1. Introduction

Sand dunes are ubiquitous in natural subaqueous environments (Best, 2005). Understanding their dynamics is important for many areas such as the offshore industry, navigation, or marine renewable energies (Barrie et al. 2005). Sand dunes in coastal areas present a high degree of heterogeneity, which is due to the spatio-temporal variability of forcing conditions, the type and quantity of sediment, and a history of evolution (Rubin and McCulloch 1980; Belderson et al. 1982; Li et al. 2014). Dune geometrical dimensions are linked to the water depth, D (Charru, 2013). Dune wavelengths are of the order of tens of meters and heights of a few meters in tidal channels of depth of the order of tens of meters (Thauront, 1995; Ernstsens et al., 2006). At the scale of a tidal cycle, the dune profile will adapt to the quick variations of the current intensity and the water depth, between two slack tides. Some authors measured horizontal dune crest displacements up to three meters and vertical displacement of a few tens of centimeters, at depths around fifteen meters, in tidal environments (Langhorne, 1982; Ernstsens et al., 2006). Observation showed that dune front slopes of ebb-oriented dunes is steeper during ebb tides, with values up to 15-20°, and that a recirculation cell can develop intermittently downstream of crests (Kostaschuk and Best, 2005; Ernstsens et al., 2006; Lefebvre et al., 2013). Superimposed ripples were observed migrating on dune profiles, with varying orientation and migration rates (Knaapen et al. 2002; Ernstsens et al. 2006; Barnard et al. 2012). The morphodynamic evolution of subaqueous sand dunes has been extensively studied during controlled experiments (Coleman and Melville, 1996; Fourriere et al., 2010) or in numerical modeling studies mostly for steady current conditions (Niemann et al., 2011; Nabi et al., 2013; Dore et al., 2016). Sand dunes in tidal environments present a higher degree of complexity, and to date no numerical model exists that can simulate their evolution. In this paper, we present the results of measurements carried out in the southern pass of the Arcachon inlet, southwest France, to observe and analyze sand dune and superimposed ripple dynamics for two tidal cycles. Then, we introduce a numerical model to simulate sand ripple and dune dynamics submitted to a tidal current, and we present the results for several tidal cycles.

2. Observation of sand dune dynamics over a tidal cycle

2.1 Situation and study area

The Arcachon lagoon is situated on the southwest coast of France and communicate with the Atlantic Ocean through a tidal inlet of an average width of 3 kilometers (figure 1). The tidal range varies from 0.8 m to

¹Danish Hydraulics Institute, Agern Allé 5, 2970 Hørsholm, DANEMARK. ard@dhigroup.com

² Université de Bordeaux, CNRS; UMR 5805-EPOC, Talence, F-33405, FRANCE. philippe.bonneton@u-bordeaux.fr

³ Université de Bordeaux, CNRS; UMR 5805-EPOC, Talence, F-33405, FRANCE. vincent.marieu@u-bordeaux.fr

⁴ SHOM ; HOM/REC-CFuD/Sédimentologie, CS 92803, 29228 BREST Cedex 2, France. garlan@shom.fr

4.6 m for neap and spring tides, respectively. The mouth of the lagoon has a complex and active morphology, with a vast ensemble of sand banks, fed by an important southward littoral drift and shaped by highly energetic waves. The tidal inlet is composed of a northern and a southern channel, with maximum depth averaged current velocities up to $2 \text{ m} \cdot \text{s}^{-1}$ and $1.4 \text{ m} \cdot \text{s}^{-1}$, respectively (Pedreros et al. 2008). The study area is located in the southern pass, between a sand bank (Arguin sand bank) and the southern shore of the inlet. Thauront (1995) conducted lateral sonar measurements and observed the presence of sand dunes on the bottom of both inlets. The area is rich in non-cohesive sediment, with strong tidal currents, and is sheltered from the waves, insuring mostly unidirectional tidal forcing conditions. The bottom of the southern pass was also well preserved from human intervention (Doré, 2015).

2.2 Material and methods

We carried out seven measurements campaigns in the inlet of the Arcachon lagoon between April 2013 and June 2014. We used an echosounder linked to a GPS to measure bathymetry transects in the study area at different dates. A pre-selected dune profile was measured during two tides of different intensity, for the mean tide of September 14, 2013, and the spring tide of June 13, 2014, to evaluate dune and superimposed ripple short term dynamics. We measured current velocities along the dune profile with a ship mounted ADCP. An ultrasound altimeter ALTUS was deployed on the dune profile to detect the migration of superimposed bedforms. We placed a tripod structure mounted with an ADCP and an ADV close to the dune crest to measure boundary layer currents for a full spring-neap tidal cycle. The experimental design is shown on figure 2.

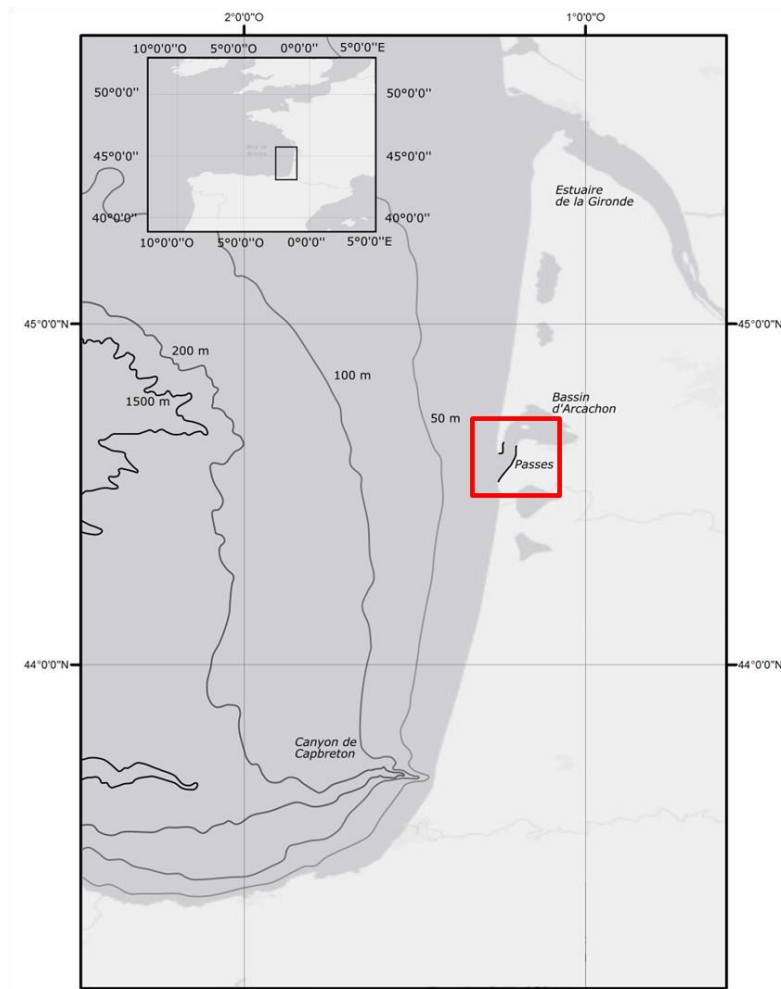


Figure 1. Localization of the study area in southwest France (red square).

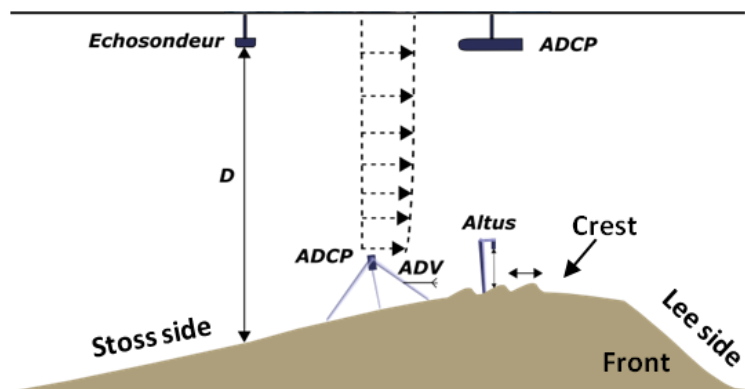


Figure 2. Sketch of the experimental design with the instruments deployed during measurement campaigns.

2.3 Bathymetry

The bathymetry was first measured over a large area during three preliminary campaigns, between April 22nd, 2013 and July 08th, 2013. The interpolated data showed a field of large bedforms with crests spaced by several tens of meters and covering the sandy bottom. Bedforms in the southern pass have asymmetrical profiles oriented towards the south west, in the ebb flow direction. Crest heights of a couple of meters gradually decrease from the middle of the channel towards the edges, where the positions of the crests are also more advanced and more spaced. A Fourier spectral analysis of the bottom revealed two main peaks of energy around $\lambda = 70\text{ m}$ and $\lambda = 105\text{ m}$, λ being the wavelength, in the middle and in the edges of the channel, respectively (Doré, 2015). Considering a mean water depth of $\bar{D} = 13\text{ m}$, these wavelengths correspond to values of the adimensional depth $k\bar{D}$ around unity, k being the wave number, which is the signature of a dune mode (Fourrière, 2010). The lower and more spaced dune crests in the channel edges are characteristic of a milieu that is poorer in sediment (Dréano, 2010; Li, 2014). The bathymetry was measured again on September 13th, 2013 on a smaller area to select a dune profile and study its dynamics (figure 3).

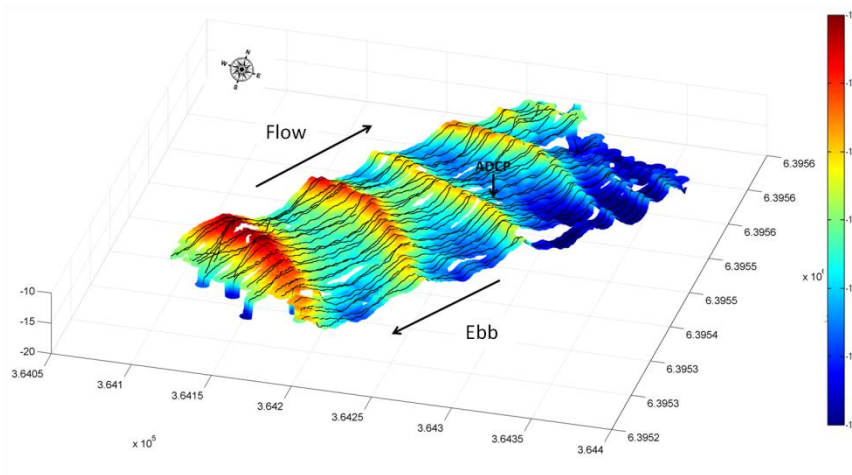


Figure 3. Bathymetry on September 13th, 2013. The position of the ADCP is showed on the selected dune profile.

2.4 Results

The dune profile was observed for a tide of moderate tidal range (mean tide), on September 24th, 2013 (figure 4), and for a spring tide on June 13th, 2014 (figure 5).

Measurements carried out during the mean tide of September 24th covered the second half of the ebb tide (3 hours before low tide) and the beginning of the flow. Figure 4 shows the position of the crest, C , and of a

superimposed ripple, R , located close to the trough. R is clearly changing polarity between the ebb and the flow phases. The weak migration rate of R could not be assessed. The dune profile keeps an asymmetry in the direction of the ebb tide, even during the flow tide. The dune front has a gentle slope of around 5° , which is weakly varying during the tidal cycle. The profile is bended on the stoss side, mostly during the flow, between $x = 70\text{ m}$ and $x = 80\text{ m}$, x being the abscissa perpendicular to the dune front. This ‘cat-back’ shaped dune profile has already been described by Langhorne (1982), but is not well understood. The profile slope in the vicinity of the crest on the dune stoss side is higher than 15° during the flow, which is above the threshold value for the existence of a flow recirculation cell (Paarlberg et al., 2009). Such a recirculation cell possibly enhances locally the steepening of the profile on the stoss side. During the period of measurement, the dune crest is moving in the direction of the inlet axis with an average velocity of $0.5\text{ m}\cdot\text{h}^{-1}$, during ebb tide, and $0.4\text{ m}\cdot\text{h}^{-1}$, during flow tide, leading to horizontal displacements of $\Delta x = -1.55\text{ m}$ and $\Delta x = 0.6\text{ m}$, during ebb and flow tide, respectively. Integrating the mean migration rate over the full duration of the ebb and flow tides gives a mean amplitude of the crest horizontal displacement of the order of $|\Delta x| \sim 2.8\text{ m}$ during the tidal cycle.⁵

The red dotted line on figure 4 shows the time when the suspended sediment transport, q_s , has become negligible, around 1h45 pm, due to a reduced mean tidal current velocity⁶. After that time, the crest stabilizes and starts moving backwards until low tide, around 3 pm. The crest is also moving in the vertical plane (not shown here), with displacements of $\Delta z = -10\text{ cm}$ before 1h45 pm, and then is increasing of $\Delta z = 10\text{ cm}$ after that time (Doré, 2015). This means that the displacement of the crest, between 1h45 pm and 3 pm, in the opposite direction of the ebb flow, is probably due to the adaptation of the dune profile to milder sediment fluxes conditions, in absence of suspended sediment fluxes that usually flatten the dune profile shape. After 3pm, the flow is inverting and the crest is slowly moving in the direction of the flow.

Measurements during the spring tide of June 13th, 2014 started at 7h30, 1.5 hours after high tide. Figure 5 shows the position of the crest, C , and of four superimposed ripple, noted $R1$ to $R4$. $R1$ to $R3$ are located on the dune stoss side, whether $R4$ is located on the dune front slope. The dune crest is moving horizontally over a distance of $\Delta x = -2.44\text{ m}$, at an average rate of $0.65\text{ m}\cdot\text{h}^{-1}$. Assuming that the mean migration rate during the measurement period is equal to the mean migration rate for the full ebb tide, leads to a total crest displacement of $\Delta x = -3.8\text{ m}$. In the meantime, the vertical position of the dune crest is decreasing by $\Delta z = -0.3\text{ m}$ (not shown here), due to important suspended sediment fluxes, a consequence of relatively high current velocities.⁷ The dune profile for mean tide conditions is represented on top of the profile for the spring tide on figure 5. During the spring tide, the dune profile asymmetry is strongly marked in the direction of the ebb flow, whether during the mean tide, the profile is less asymmetric. The larger magnitude of the sediment transport in suspension during the spring tide flattens the dune profile.

Superimposed ripples have wavelengths between 5 to 17 meters and heights between 0.15 m to 0.6 m, $R1$ being the smallest and $R3$ being the largest. $R1$ to $R3$ are migrating in the direction of the crest, with migration velocities between $0.3\text{ m}\cdot\text{h}^{-1}$ and $0.5\text{ m}\cdot\text{h}^{-1}$, respectively closer to the trough ($R1$) and higher on the dune profile ($R3$). $R4$ is migrating in the opposite direction of the ebb current until 9h30, then is changing polarity and start migrating in the direction of the ebb current (figure 5). This is the signature of a flow recirculation cell in the lee of the dune front, which was also confirmed by ADCP measurements over the dune front slope around mid ebb tide (Doré, 2015). Ripple heights are varying between measurements with amplitudes up to $\Delta z = 4\text{ cm}$, 9 cm and 15 cm for $R1$ to $R3$, respectively. As the tide is changing direction around 11h30, ripples are changing polarity and start moving in the direction of the flow (figure 5).

Superimposed ripples were also observed in the vicinity of the dune crest with an ALTUS, which was able to detect the oscillating movement of ripple crests under the sensor during several tidal cycles, leading to

⁵ We assumed that the crest migration rate during the first 2.5 hours (1.5 h) and the last 3 hours (5 h) of the ebb (flow) tide is conserved, leading to $\Delta x = 2.9\text{ m}$ during ebb tide and $\Delta x = 2.6\text{ m}$ during flow tide, respectively. Δx is therefore underestimated for the flow tide.

⁶ At that time $U < 0.7\text{ m}\cdot\text{s}^{-1}$, U being the mean tidal current velocity (Doré, 2015).

⁷ $U > 0.7\text{ m}\cdot\text{s}^{-1}$ until 11h20 (Doré, 2015).

similar values of ripple migration rates (Doré, 2015; Doré et al., 2017).

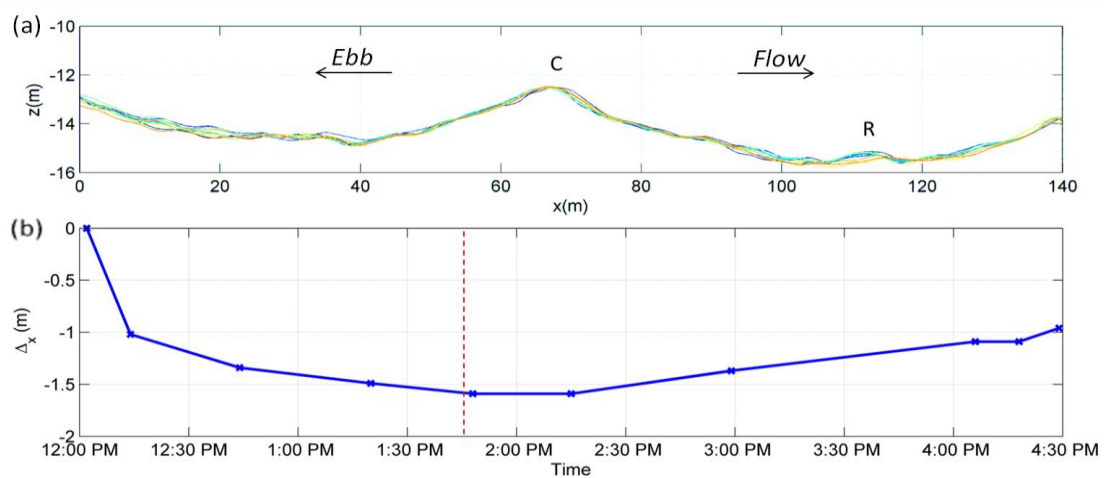


Figure 4. a) Dune profile evolution during the mean tide of September 24, 2013. 'C' stands for the crest, and 'R' for a superimposed ripple in the bottom part of the dune profile. The color palette from blue to red describes transects at different times of the tidal phase, from the oldest to the newest. (b) Relative horizontal displacement of the dune crest. The red dotted line corresponds to the date when q_s becomes negligible.

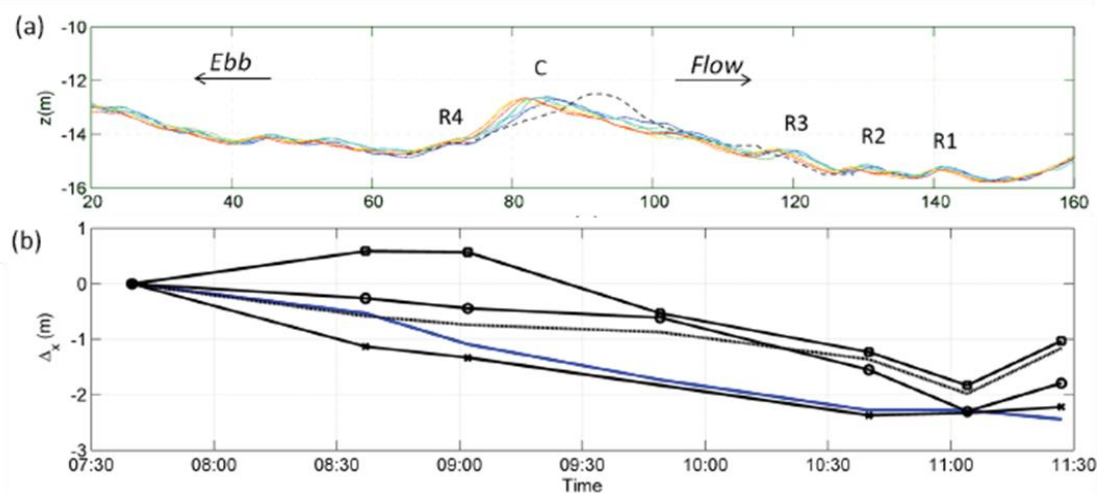


Figure 5. (a) Dune profile evolution during the spring tide on June 13, 2014. 'C' stands for the crest, and 'R1' to 'R4' for the superimposed ripples. The color palette from blue to red describe transects at different times of the tidal phase, from the oldest to the newest. The dotted line represents the dune profile for the mean tide on September 24, 2013. (b) Relative horizontal displacement of dune and ripple crests. Blue : C; black, --: R1; o- : R2; x- : R3; □- : R4.

3. Numerical modeling of tidal sand dune dynamics

We apply the model of Doré et al. (2016) that successfully reproduced the morphodynamic evolution of sand dunes under steady current conditions. We adapted the model to take into account tidal forcing conditions.

3.1 Numerical model and parameters

The model solves the Reynolds Averaged Navier Stokes equations in the boundary layer and the turbulence field is calculated with a $k-\omega$ scheme (Andersen, 1999). The sediment transport module calculates the bedload flux using the formulation of Meyer-Peter and Müller (1948) and the suspended sediment

concentration is calculated through an advection-diffusion equation with the bottom concentration calculated from the formulation of Engelund and Fredsøe (1976). The morphological module was developed by Marieu et al. (2008) and is particularly suited to handle fluxes discontinuities at the crests. The hydrodynamic and morphological modules are decoupled considering that the adaptation time of the hydrodynamic is small compared to the bed evolution time. The morphological module time step is adjusted during the simulation to avoid the occurrence of numerical spurious oscillations.

In order to insure realistic simulations, we extracted the forcing conditions from *in situ* ADCP and ADV measurements above the dune profile. The free surface is represented by a rigid lid in the model, therefore the discharge was adjusted to retrieve the bottom shear velocity, u^* , assuming a logarithmic profile of the current velocity in the boundary layer, and integrating over the depth. At the bottom boundary, the *in situ* sand roughness, $k_n = 7.75 \cdot 10^{-4} m$, is used. The simulation starts at mid-flow-tide of the first spring tide in the measurements. In the simulations the flow (ebb) tide is conventionally directed towards the positive (negative) abscissa.

Two modeling scenarios were carried out. In the first scenario, *R*, the bed evolution is simulated starting with a slightly perturbed, quasi-flat bed. The bed evolution encompasses various orders of magnitudes of bedform wavelengths ($\langle \lambda \rangle \sim 0.08 m$ to $\langle \lambda \rangle \sim 17 m$) and therefore five numerical models with different domain resolutions are used⁸ to avoid prohibitive calculation times (table 1). In the second scenario, *D*, the bottom is covered with dunes of the same size as the dunes observed *in situ* ($\langle \lambda \rangle \sim 70 m$ and $\langle H \rangle \sim 2 m$). The calculation domain has the same characteristics as domain 5 in table 1. Ripple wavelengths and heights are retrieved using the autocorrelation of the bed profile during the incipient ripple generation phase, and using a zero crossing approach at a later stage during the non-linear bed development phase (Doré et al., 2016).

Table 1. Parameters used for the simulation of scenario *R*. t_i : initial time, N_x : number of grid points in the horizontal direction, L : domain length, H_f , λ_f : mean ripple height and wavelength at the end of the simulation.

Domain	t_i	N_x	L	H_f	λ_f
1	0	400	2.3	0.015	0.3
2	330	800	12	0.025	0.55
3	430	500	12	0.06	1.1
4	980	400	12	0.26	5.2
5	21500	800	140	0.6	17

3.2 Results

3.2.1 Evolution of the quasi flat bed

The results show a rapid evolution of the small perturbations in the first instants of the evolution (figure 6a), with a rapid growth of the bed height and the emergence of ripples with a preferred wavelength, similar to the incipient ripple generation under steady current conditions (Doré et al., 2014; Doré et al., 2016). Migration velocities are decreasing until $t = 10,000 s$, at high tide, due to weaker current intensities and larger bedform that have lower migration velocities. Bedforms lose their asymmetry and change of polarity around $t = 13,000 s$, as currents are reversing and increasing in the opposite direction (figure 6b). The above described dynamics is repeated along tidal cycles as shown on figure 7. Ripples are merging the ones with the others, mostly at mid-ebb tide and mid-flow tide, when currents have the highest intensities. Merging sequences lead to an increase of both ripple heights and lengths, as already described for steady current conditions (Doré et al., 2016) and their number is accordingly decreasing. The time evolution of ripple statistical mean height, $\langle H \rangle$, and wavelength, $\langle \lambda \rangle$, are shown on figure 8. The curve of ripple height evolution clearly show an alternance of phases of increase, around mid-tides, and phases of relative stability around slack tides. The periods of increase in mean ripple height correspond to cascading merging sequences

⁸ A resolution of 30-40 grid points per wavelength is recommended (Doré et al., 2016).

that are clearly visible on figure 7. Wavelengths are also increasing, but with a time lag compared to heights, as they slowly adapt to the higher heights of the merged ripples ($t < 60,000$ s, figure 8).

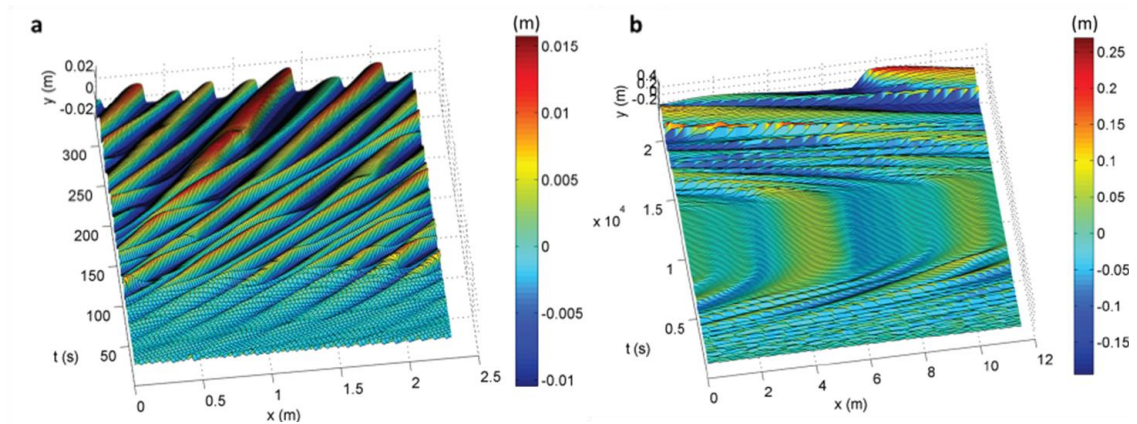


Figure 6. Time evolution of bed height for $0 < t < 330$ s, domain 1 (a) and $330 < t < 21,500$ s, domain 2-4 (b).

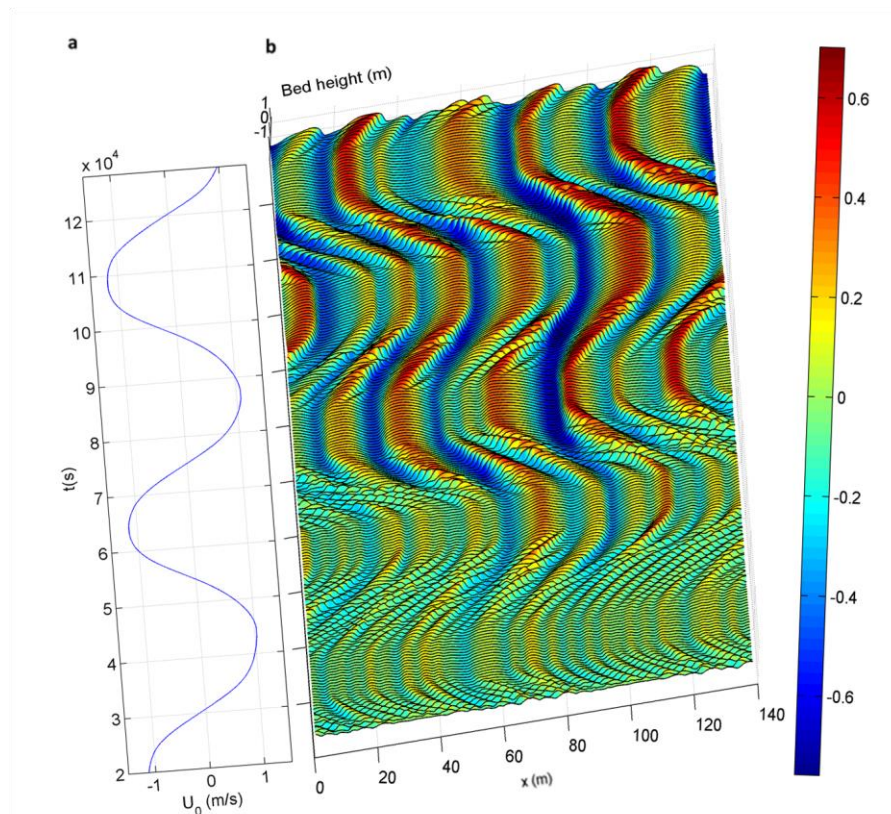


Figure 7. Time evolution of the mean current velocity (a) and of the bed height (b) for $t > 21,500$ s, domain 5.

Beyond the brief incipient ripples generation phase, which is characterized by an exponential growth (Doré et al., 2016), both curves of $\langle H \rangle$ and $\langle \lambda \rangle$ show two distinct phases of evolution. During the first 5.5 hours ($t < 20,000$ s), the time evolution of both statistical wave height and wavelength can be approximated by the unified relation for bedform development of Perillo et al. (2014), as follows⁹:

$$\langle \lambda, H \rangle = \langle \lambda_{t5.5}, H_{t5.5} \rangle (1 - e^{-C_{\lambda,h}t}), \quad (1)$$

⁹ Trend lines are chosen in order to fit the values of mean wavelengths and heights around mid-tide.

$\langle \lambda_{t5.5}, H_{t5.5} \rangle$ being the bedform statistical mean wavelength and height at $t = 20,000$ s. C_λ and C_h are calibrating coefficients for wavelength and height evolution, respectively¹⁰. For $t > 20,000$ s, a relation similar to equation 1 would overestimate the bed evolution, which is better approximated by the following logarithmic relation :

$$\langle \lambda, H \rangle = \langle \lambda_e, H_e \rangle (\alpha \ln(t) - 1), \quad (2)$$

$\langle \lambda_e \rangle$ and $\langle H_e \rangle$ being the statistical mean wavelength and height at equilibrium, respectively, with $\langle \lambda_e \rangle = 70$ m and $\langle H_e \rangle = 2.2$ m, in agreement with *in situ* values, and $\alpha = \frac{2}{\ln(T_e)} = 0.11$, T_e being the time to equilibrium. Equation 1 corresponds to a situation when frequent merging sequences occur wether equation 2 accurately represents the bottom evolution when merging sequences are more scarce and bedform growth is mostly linked to sediment fluxes intensity. Equation 2 gives an equilibrium time of $T_e = 2.5$ years. T_e is in good agreement with the time that would be required to generate a dune of equivalent volume taking into account the net sediment fluxes measured *in situ* on the dune profile (Doré et al., 2017).

Ripple mean statistical height and wavelength reach values of $\langle H \rangle = 0.6$ m (0.3 m) and $\langle \lambda \rangle = 17$ m (8 m) after a time interval of 35 hours (15 hours). These values correspond to wavelengths and heights of superimposed ripples observed *in situ* on the dune stoss side and in the dune trough (figure 5). Modeled ripple heights show variations in amplitude up to $\Delta z = 15$ cm between mid-tides and slack-tides (figure 8), which are of the same order of magnitude as variations measured *in situ* (section 2.4).

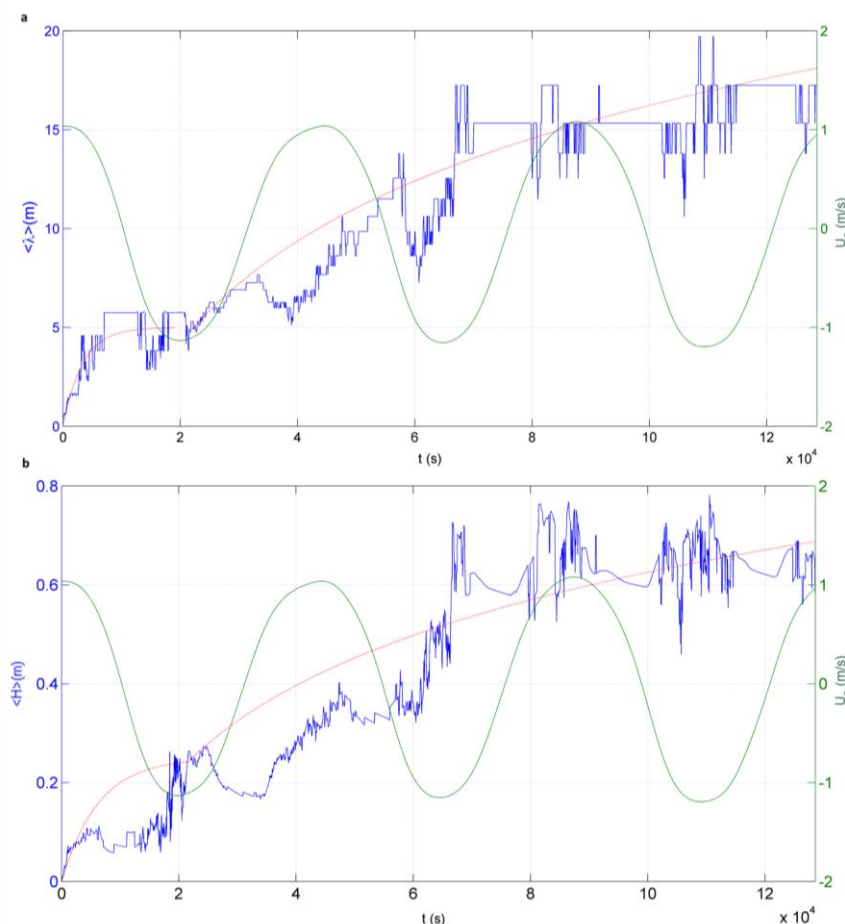


Figure 8. Time series of the statistical mean ripple wavelength (a) and height (b) for the full simulation. The red dotted curves represent equation 1 ($t < 20,000$ s) and equation 2 ($t > 20,000$ s).

¹⁰ $C_\lambda = 0.0003$ and $C_h = 0.00016$

3.2.2 Large dune dynamics over several tidal cycles

In scenario *D*, we use the numerical model to simulate the dynamics of larger dunes forced by a tidal current. The forcing conditions are the same as in scenario *R*. A parametric study to test the effects of the bed roughness on the bed evolution was carried out. The results show that for lower bed roughness values in the range $k_n = 1 - 2.5 d_{50}$, dune crests have large horizontal movements leading to changes of polarity of dune profiles, which is not observed *in situ*. Modeled dune heights are also increasing to much larger values than in the observations. For $k_n > 20 d_{50}$, the modeled dune field is quickly eroded and modeled dune heights are much lower than observed dune heights. A bed roughness of $k_n = 10 d_{50}$ was finally used in the simulation to model the drag effects due to roughness elements that are present on the dune profile. The sand surface roughness is used to calculate the sediment fluxes, which are calibrated by comparing with values measured at the dune crest.

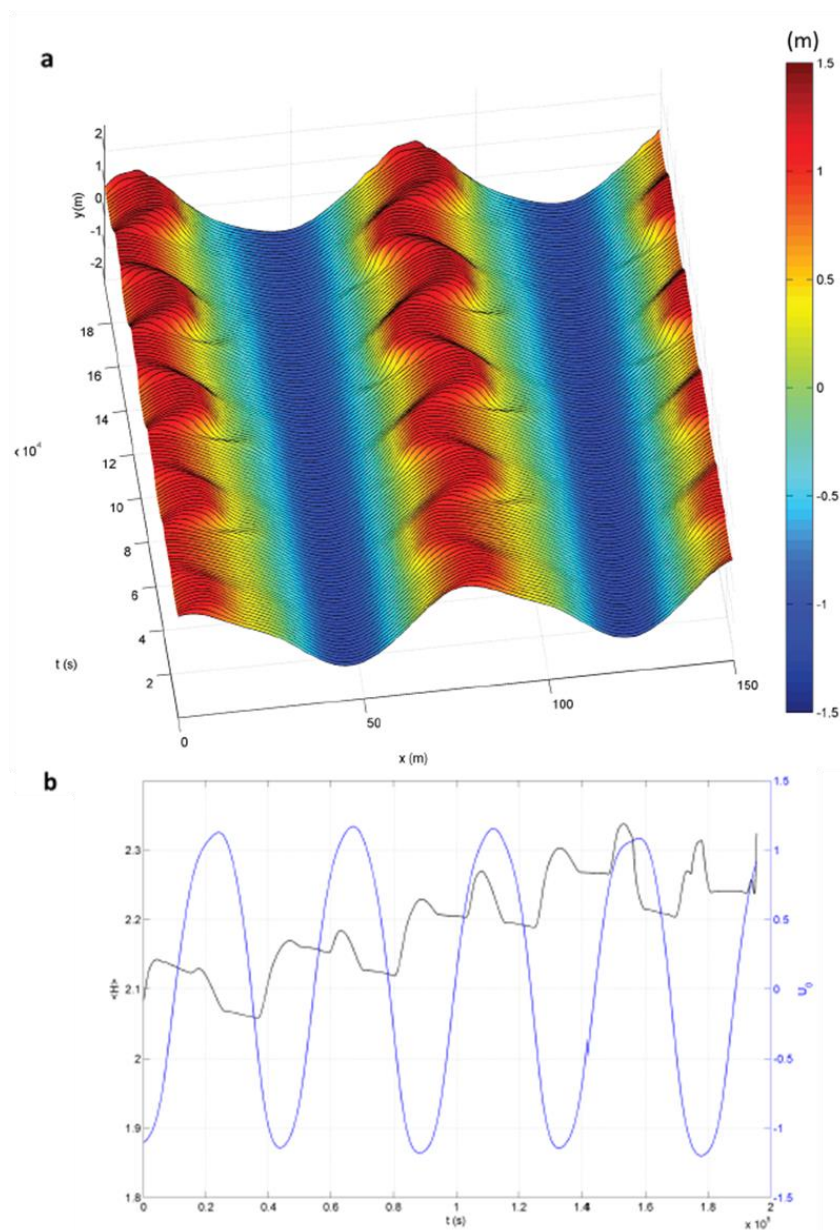


Figure 9. (a) Time evolution of the of the bed height. (b) Time series of the mean dune height (black) and of the mean tidal current velocity (blue) for $0 < t < 190,000$ s.

Figure 9a shows the time evolution of the dune field over several tidal cycles, and figure 9b shows the time evolution of dune statistical mean height against the mean tidal current velocity. Ebb (flow) currents are directed to the left (right).

The results show that the dune field is slowly migrating in the direction of the ebb flow, which is also the direction of the net sediment transport (Doré et al., 2017). Dune crests are oscillating between ebb and flow phases but keep their asymmetry in the direction of the ebb flow. Crest horizontal displacements of a few meters are of the same order of magnitude as in the observations. During the first hours of flow phases, the dune profile is bended on the stoss side (around $x = 100\text{ m}$, figure 9a), reproducing the ‘cat back’ dune profile shape in agreement with observations (section 2.4). Dune heights are generally larger during the flow (figure 9b), due to higher bottom shear stresses values during ebb tide, a consequence of lower water depths and slightly higher mean flow velocities. The modeled vertical displacements of dune crests of a few tens of centimeters during a tidal cycle (figure 9b) are of the same order of magnitude as the ones measured *in situ* (section 2.4).

4. Conclusion

A series of measurements were carried out in the tidal inlet of Arcachon, southwest France, to observe short term dune dynamics. The bathymetry revealed that the bottom is covered by a field of tidal sand dunes with an average wavelength of five to eight times the mean water depth. The measurements showed that dune profiles have a strong dynamics over the tidal cycle, oscillating horizontally with an amplitude of a few meters, and moving vertically with an amplitude of a few tens of centimeters. We observed superimposed ripples migrating on the studied dune profile with velocities of a few tens of centimeters per hour, and changing polarity between ebb and flow tidal phases. A 2D RANS model was used to simulate the evolution of an erodible non-cohesive sand bed forced by tidal currents. The model accurately reproduced the generation of ripples with wavelengths and heights of the same order of magnitude as superimposed ripples observed *in situ*, and with a similar dynamics linked to the tidal currents. The model was used to model the dynamics of a field of large sand dunes and results showed good agreement with the measurements. The results open promising perspectives for numerical modeling of tidal sand dune evolution.

Acknowledgements

This research is supported by the SHOM (Service Hydrographique de la Marine) under the research contract 12CR4. The deployment of the echosounder and the GPS was financed by the DRONEO project (EPOC/CNRS).

References

- Andersen, K. H. (1999). “The dynamics of ripples beneath surface waves and topics in shell models of turbulence”, Ph.D. dissertation, Det Naturvidenskabelige Fakultet Københavns Universitet.
- Barnard, P. L., L. H. Erikson, D. M. Rubin, P. Dartnell, et R. G. Kvittek, 2012. Analyzing bedforms mapped using multibeam sonar to determine regional bedload sediment transport patterns in the san francisco bay coastal system, *Marine Geology*, 2012, doi :10.1016/j.margeo.2012.10.011.
- Barrie, J. V., P. R. Hill, K. W. Conway, K. Iwanowska, et K. Picard, Georgia basin : Seabed features and marine geohazards, *Geoscience Canada*, 32, 145-156, 2005.
- Belderson, R. H., M. A. Johnson, et N. H. Kenyon, Bedforms, 27-57 pp., London : Chapman and Hall, 1982.
- Best, J., The fluid dynamics of river dunes: A review and some future research directions, *Journal of Geophysical Research*, 110, F04S02, 2005, doi :10.1029/2004JF000218.
- Charru, F. (2013), Sand ripples and dunes, *Annual Review of Fluid Mechanics*, 45, 469-493, doi:10.1146/annurev-fluid-011212-140806.

- Doré, A., P. Bonneton, V. Marieu, et T. Garlan, Modélisation de l'évolution morphodynamique des dunes sous-marines, *Proceedings des XIII èmes JNGCGC*, Dunkerque 2-4 Juillet 2014, 289-296, 2014, doi :10.5150/jngegc.2014.032.
- Doré, A., Modélisation de l'évolution morphodynamique des dunes sous-marines, *Ph.D. dissertation*, Ecole Doctorale Sciences de l'Environnement de l'université de Bordeaux, 2015.
- Doré, A., P. Bonneton P., V. Marieu, T. Garlan, 2016. Numerical modeling of subaqueous sand dunes morphodynamics, *J. Geophys. Res. Earth Surf.*, 121, 565-587, doi: 10.1002/2015JF003689.
- Doré, A., P. Bonneton P., V. Marieu, T. Garlan, 2017. Observation and analysis of tidal dune dynamics in the Arcachon inlet (bay of Biscay), *in prep.*
- Dreano, J., A. Valance, D. Lague, et C. Cassar, Experimental study on transient and steady-state dynamics of bedforms in supply limited configuration, *Earth Surface Processes and Landforms*, 35, 1730-1743, 2010, doi :10.1002/esp.2085.
- Engelund, F., and Jorgen Fredsoe, A sediment transport model for straight alluvial channels, *Nordic Hydrology*, 7, 293-306, 1976.
- Ernstsen, V. B., R. Noormets, C. Winter, D. Hebbeln, A. Bartholoma, B. W. Flemming, et J. Bartholdy, Quantification of dune dynamics during a tidal cycle in an inlet channel of the Danish Wadden Sea, *Geo-Marine Letters*, 26, 151-163, 2006, doi :10.1007/s00367-006-0025-3.
- Flemming, B. W., et R. A. Davis, Dimensional adjustment of subaqueous dunes in the course of a spring neap semicycle in a mesotidal backbarrier channel environment (german wadden sea, southern north sea), *Proc 3rd Int Res Symp Modern and Ancient Clastic Tidal Deposits*. Senckenberg Institute, Wilhelmshaven, Germany, 28-30, 1992.
- Knaappen, M. A. F., C. N. Van Bergen Henegouw, et Y. Y. Hu, Quantifying bedform migration using multi-beam sonar, *Geo-Marine Letters*, 46, 2002.
- Kostaschuk, R., and J. Best (2005), Response of sand dunes to variations in tidal flow : Fraser estuary, Canada, *Journal of Geophysical Research*, 110, F04S04, doi:10.1029/2004JF000176.
- Langhorne, D. N., A study of the dynamics of a marine sandwave, *Sedimentology*, 29, 571-594, 1982.
- Lefebvre, A., V. B. Ernstsen, and C. Winter (2013), Estimation of roughness length sand flow separation over compound bedforms in a natural tidal inlet, *Continental Shelf Research*, 61-62, doi:10.1016/j.csr.2013.04.030.
- Li, M. Z., J. S. Shaw, B. J. Todd, V. E. Kostylev, et Y. Wu, Sediment transport and development of banner banks and sandwaves in an extreme tidal system : Upper bay of Fundy, Canada, *Continental Shelf Research*, 83, 86-107, 2014, doi :10.1016/j.csr.2013.08.007.
- Marieu V., Bonneton P., Foster D. L. and Arduhin F. (2008). Modeling of vortex ripple morphodynamics. *Journal of Geophysical Research*, 113, C09007.
- Nabi, M., H. J. D. Vriend, E. Mosselman, C. J. Sloff, and Y. Shimizu (2013). Detailed simulation of morphodynamics: 3. ripples and dunes, *Water Resources Research*, 49, 1-14, doi:10.1002/wrcr.20457.
- Niemann, S. L., J. Fredsoe, and N. G. Jacobsen, Sand dunes in steady flow at low Froude numbers : dune height evolution and flow resistance, *Journal of Hydraulic Engineering*, 137, 5-14, 2011.
- Pedreras, R., S. Lecacheux, A. Sottolichio, E. Romieu, D. Idier, P. Salles, et M. Delattre, 2008. Caractérisation des vagues dans les passes du bassin d'Arcachon, *Proceedings des Xèmes JNGCGC*, Sophia Antipolis 14-16 Octobre 2008, 273-282, doi :10.5150/jngegc.2008.026-P.
- Rubin, D. M., et D. S. McCulloch, Single and superimposed bedforms : a synthesis of San Fransisco bay and flume observations, *Sedimentary Geology*, 26, 207-231, 1980.
- Thauront, F., Les transits sédimentaires subtidaux dans les passes internes du bassin d'Arcachon, *Ph.D. dissertation*, Université de Bordeaux 1, 1995.
- Todd, B. J., Morphology and composition of submarine barchan dunes on the scotian shelf, canadian atlantic margin, *Geomorphology*, 67, 487-500, 2005, doi :10.1016/j.geomorph.2004.11.016.